Journal of Computational Physics 228 (2009) 3345–3357

Contents lists available at ScienceDirect

Journal of Computational Physics

journal homepage: www.elsevier.com/locate/jcp

Numerical solution of the linearized Boltzmann equation for an arbitrary intermolecular potential

Felix Sharipov *, Guilherme Bertoldo

Departamento de Física, Universidade Federal do Paraná, Caixa Postal 19044, Curitiba, 81531-990, Brazil

ARTICLE INFO

Article history:
Received 11 October 2008
Accepted 20 January 2009
Available online 29 January 2009

PACS:
51.10.+y
51.20.+d
47.45.−n

Keywords:
Boltzmann equation
Discrete velocity method
Differential cross section
Heat conductivity
Viscosity

ABSTRACT

A numerical procedure to solve the linearized Boltzmann equation with an arbitrary intermolecular potential by the discrete velocity method is elaborated. The equation is written in terms of the kernel, which contains the differential cross section and represents a singularity. As an example, the Lennard-Jones potential is used and the corresponding differential cross section is calculated and tabulated. Then, the kernel is calculated so that to overcome its singularity. Once, the kernel is known and stored it can be used for many kinds of gas flows. In order to test the method, the transport coefficients, i.e. thermal conductivity and viscosity for all noble gases, are calculated and compared with those obtained by the variational method using the Sonine polynomials expansion. The fine agreement between the results obtained by the two different methods shows the feasibility of application of the proposed technique to calculate rarefied gas flows over the whole range of the Knudsen number.

1. Introduction

Nowadays, most of problems of rarefied gas dynamics are solved on the basis of the model kinetic equations. Many examples of such an approach can be found e.g. in Refs. [1–3]. The model equations are obtained as a simplification of the exact Boltzmann equation. As a result, they reduced significantly computational efforts to calculate rarefied gas flows and became a widely used tool in practical calculations. However, the simplification introduces an uncertainty, which can be estimated only if a numerical solution based on the exact Boltzmann equation is available at least for few values of the main parameter of rarefied gas dynamics, viz. Knudsen number.

Recently, the interest to weakly disturbed rarefied gas flows increased because of their applications to microfluidics, see e.g. Ref. [4]. The fact is that, the weakly disturbed gas flows cannot be calculated by the direct simulation Monte Carlo method [5], but the linearized kinetic equation should be applied. In this connection, here we will restrict ourselves only by the linearized Boltzmann equation (LBE).

A numerical solution of the LBE represents great computational difficulties related to calculations of the collision operator, which is a five fold integral in general case. If one assumes the hard sphere model for the intermolecular interaction, then the collision integral can be simplified and reduced to a four fold integral. An application of the LBE to one-dimensional flows

* Corresponding author. Tel.: +55 4133613337; fax: +55 4133613418.
E-mail addresses: sharipov@fisica.ufpr.br (F. Sharipov), glbertoldo@gmail.com (G. Bertoldo).
URL: http://fisica.ufpr.br/sharipov (F. Sharipov).

0021-9991/$ - see front matter © 2009 Elsevier Inc. All rights reserved.
doi:10.1016/j.jcp.2009.01.016

allows to reduce the collision operator to a three fold integral. Because of this simplification the LBE for the hard spheres was successfully applied to obtain the transport coefficients [6–9] and to calculate some one-dimensional flows Refs. [10–23].

Although the above cited works represent a remarkable advance in the numerical solution of the LBE, they are restricted by the hard sphere model of the molecular interaction. At the same time, some investigations, Refs. [24,25], showed that the intermolecular potential can strongly influence some phenomena in rarefied gases. That is why, it is very important to elaborate numerical technique to solve the LBE for an arbitrary potential. The main difficulties of such a technique are related to calculations of the collision operator, which contains a singular kernel. Moreover, the calculation of the kernel itself depends on the differential cross section, which in general case is not an analytic function and must be calculated numerically.

The aim of this work is to elaborate a numerical technique to calculate the collision operator with the singular kernel assuming an arbitrary intermolecular potential. To demonstrate an application of the presented techniques, the thermal conductivity and viscosity coefficients are calculated for the (6–12) Lennard-Jones potential.

2. Statement of the problem

In the linear theory, the gas is assumed to be weakly disturbed from its equilibrium state described by the Maxwellian distribution function

$$f_0(\boldsymbol{v}) = \frac{n}{(\sqrt{\pi}v_m)^3}\exp\left[-\left(\frac{v}{v_m}\right)^2\right], \quad v_m = \left(\frac{2kT}{m}\right)^{1/2}, \tag{1}$$

where n is the equilibrium number density, T is the equilibrium temperature, $\boldsymbol{v}$ the molecular velocity, v_m is the most probable molecular speed, m is the molecular mass, and k is the Boltzmann constant. The non-equilibrium distribution function $f(\boldsymbol{r}', \boldsymbol{v})$ is related to the perturbation function $h(\boldsymbol{r}', \boldsymbol{v})$ as

$$f(\boldsymbol{r}', \boldsymbol{v}) = f_0(\boldsymbol{v})[1 + h(\boldsymbol{r}', \boldsymbol{v})\,\xi], \tag{2}$$

where ξ is a small parameter of linearization and $\boldsymbol{r}'$ is the spacial position vector. In general case, the distribution function depends also on time. However, for our purpose it is enough to consider time independent problems. Substituting Eq. (2) into the full Boltzmann equation, its linearized form is obtained, see e.g. Refs. [26–29],

$$\boldsymbol{v}\cdot\frac{\partial h(\boldsymbol{r}', \boldsymbol{v})}{\partial \boldsymbol{r}'} = \widehat{L}'(h), \tag{3}$$

where $\widehat{L}'$ is the linearized collision operator. If the total cross section σ'_{T} of the interacting particles is finite, the collision integral can be split as

$$\widehat{L}'(h) = \int f_0(\boldsymbol{v}^*)K'(\boldsymbol{v}, \boldsymbol{v}^*)h(\boldsymbol{r}', \boldsymbol{v}^*)\,\mathrm{d}\boldsymbol{v}^* - \nu'(\boldsymbol{v})h(\boldsymbol{r}', \boldsymbol{v}), \tag{4}$$

where $K'(\boldsymbol{v}, \boldsymbol{v}^*)$ is the kernel given as

$$K'(\boldsymbol{v}, \boldsymbol{v}^*) = 2\pi g'\int_0^{\pi}\exp\left[-\left(\frac{g'\cot\frac{\chi}{2}}{v_m}\right)^2\right]I_0\left(\frac{2|\boldsymbol{v}\times\boldsymbol{v}^*|\cot\frac{\chi}{2}}{v_m^2}\right)\left[\sigma'\left(\frac{g'}{\sin\frac{\chi}{2}}, \chi\right) + \sigma'\left(\frac{g'}{\sin\frac{\chi}{2}}, \pi - \chi\right)\right]\frac{\sin\chi}{\sin^4\frac{\chi}{2}}\,\mathrm{d}\chi - \sigma'_{\mathrm{T}}g', \tag{5}$$

$\sigma'(g', \chi)$ is the differential cross section (DCS), $g' = |\boldsymbol{v} - \boldsymbol{v}^*|$ is the relative velocity and χ is the deflection angle depending on the impact parameter b' and on the relative velocity g', I_0 is the modified Bessel function of the first kind and zero order defined as

$$I_0(x) = \frac{1}{2\pi}\int_0^{2\pi}\exp(x\cos\zeta)\,\mathrm{d}\zeta. \tag{6}$$

The collision frequency reads

$$\nu'(v) = \sigma'_{\mathrm{T}}\int f_0(\boldsymbol{v}^*)g'\,\mathrm{d}\boldsymbol{v}^*. \tag{7}$$

Note, the total cross section σ'_{T} is related to the DCS as

$$\sigma'_{\mathrm{T}} = 2\pi\int_0^{\pi}\sigma'(g', \chi)\sin\chi\,\mathrm{d}\chi. \tag{8}$$

The DCS $\sigma'(g', \chi)$ is determined by the intermolecular interaction potential. For the hard sphere molecular it is given by the simple expression

$$\sigma' = \frac{d^2}{4}, \tag{9}$$

where d is the molecular diameter. Then, the kernel expression (5) can be significantly simplified. However, for a potential containing both attractive and repulsive forces, e.g. the Lennard-Jones one, the computation of the DCS is not trivial. As a consequence, the calculation of the kernel given by Eq. (5) becomes a very difficult task.

In the present work, a methodology of calculation of the kernel $K'(\boldsymbol{v}, \boldsymbol{v}_*)$ for an arbitrary potential will be presented and its application to the zero-dimensional problems, viz. viscosity and thermal conductivity computation, will be given. As an example the (6–12) Lennard-Jones potential [26–28] will be used, which reads

$$U'(\rho') = 4\epsilon\left[\left(\frac{d}{\rho'}\right)^{12} - \left(\frac{d}{\rho'}\right)^{6}\right], \tag{10}$$

where ρ' is the intermolecular distance, ϵ is a fixed parameter which depends on the gas species. Unlike the hard sphere model, the parameter d is not the diameter, but it corresponds to the distance with the zero potential.

As has been mentioned above, Eq. (4) is valid only for the finite total cross section. To satisfy this condition we have to restrict the range of the intermolecular influence by taking an upper limit for the impact parameter b'_{M}, which should be significantly larger than the parameter d. In this case the total cross section becomes finite and given as

$$\sigma'_{\mathrm{T}} = \pi b'^2_{\mathrm{M}}. \tag{11}$$

3. Parameterization of the problem

For the further derivations it is more convenient to introduce the following dimensionless variables

$$\boldsymbol{r} = \frac{\boldsymbol{r}'}{a}, \quad \boldsymbol{c} = \frac{\boldsymbol{v}'}{v_m}, \quad g = \frac{g'}{v_m}, \tag{12}$$

$$\rho = \frac{\rho'}{d}, \quad b = \frac{b'}{d}, \quad b_{\mathrm{M}} = \frac{b'_{\mathrm{M}}}{d}, \tag{13}$$

$$\sigma(g,\chi) = \frac{\sigma'(g',\chi)}{d^2}, \quad \sigma_{\mathrm{T}} = \frac{\sigma'_{\mathrm{T}}}{d^2} \tag{14}$$

$$U = \frac{U'}{\epsilon}, \quad E = \frac{mg'^2}{4\epsilon}, \tag{15}$$

$$\phi(\boldsymbol{c}) = \frac{v_m^3}{n} f_0(\boldsymbol{v}) = \pi^{-3/2}\mathrm{e}^{-c^2}, \tag{16}$$

where a is the characteristic size of gas flow.

In terms of the dimensionless quantities, the LBE takes the form

$$\boldsymbol{c}\cdot\frac{\partial h}{\partial \boldsymbol{r}} = ad^2 n\widehat{L}(h), \tag{17}$$

where $\widehat{L}(h)$ is the dimensionless collision operator given by

$$\widehat{L}(h) = \int \phi(\boldsymbol{c}^*)K(\boldsymbol{c},\boldsymbol{c}^*)h(\boldsymbol{r},\boldsymbol{c}^*)\,\mathrm{d}\boldsymbol{c}^* - \nu(c)h(\boldsymbol{r},\boldsymbol{c}), \tag{18}$$

$K(\boldsymbol{c},\boldsymbol{c}^*)$ is the dimensionless kernel:

$$K(\boldsymbol{c},\boldsymbol{c}^*) = 2\pi g\int_0^{\pi} \exp\left[-\left(g\cot\frac{\chi}{2}\right)^2\right] I_0\left(2|\boldsymbol{c}\times\boldsymbol{c}^*|\cot\frac{\chi}{2}\right)\left[\sigma\left(\frac{E}{\sin\frac{\chi}{2}},\chi\right) + \sigma\left(\frac{E}{\sin\frac{\chi}{2}},\pi-\chi\right)\right]\frac{\sin\chi}{\sin^4\frac{\chi}{2}}\,\mathrm{d}\chi - g\sigma_{\mathrm{T}}. \tag{19}$$

The dimensionless collision frequency $\nu(c)$ can be integrated analytically for any potential

$$\nu(c) = \frac{\sigma_{\mathrm{T}}}{\sqrt{\pi}}\left[\mathrm{e}^{-c^2} + \left(2c + \frac{1}{c}\right)\int_0^c \mathrm{e}^{-\eta^2}\,\mathrm{d}\eta\right]. \tag{20}$$

It should be noted that the collision operator has the following property:

$$\widehat{L}(\Psi) = 0, \quad \Psi = \{1, \boldsymbol{c}, c^2\}, \tag{21}$$

which is a consequence of the mass ($\Psi = 1$), momentum ($\Psi = \boldsymbol{c}$) and energy ($\Psi = c^2$) conservation laws. Using the expression of the collision operator (18) the conservations laws Eq. (21) can be also written as

$$\int \phi(\boldsymbol{c}^*)K(\boldsymbol{c},\boldsymbol{c}^*)\Psi(\boldsymbol{c}^*)\,\mathrm{d}\boldsymbol{c}^* = \nu(c)\Psi(\boldsymbol{c}). \tag{22}$$

This property can be used to overcome the singularity of the kernel $K(\boldsymbol{c},\boldsymbol{c}^*)$ arising at $g = 0$. With help of Eq. (22) the collision operator is written down as

$$\widehat{L}(h) = \int \phi(\boldsymbol{c}^*) K(\boldsymbol{c}, \boldsymbol{c}^*) \left[h(\boldsymbol{r}, \boldsymbol{c}^*) - \frac{\Psi(\boldsymbol{c}^*)}{\Psi(\boldsymbol{c})} h(\boldsymbol{r}, \boldsymbol{c}) \right] \mathrm{d}\boldsymbol{c}^*. \tag{23}$$

Although the kernel is singular at $g = 0$, the term in the brackets is zero in this limit. Such a procedure is usual in the theory of singular integral equations [30].

4. Deflection angle

The main difference of the present work from all previous ones dealt with a numerical solution of the LBE [7–9, 10–23] is the intermolecular potential with both attractive and repulsive forces. In this case the calculation of the DCS, which is a part of the kernel (19), is not so simple as that in the case of the hard sphere molecules. In this section, the numerical procedure and results on the DCS for the Lennard-Jones potential are described.

The relation of the deflection angle to the intermolecular potential can be found in many text books, see e.g. Ref. [27]. The scheme and notations for a binary collision are shown in Fig. 1.

First, the angle ψ is calculated as

$$\psi = \frac{b}{\rho_m} \int_0^1 \left[1 - \left(\frac{bq}{\rho_m} \right)^2 - \frac{U(\frac{\rho_m}{q})}{E} \right]^{-1/2} \mathrm{d}q, \tag{24}$$

where ρ_m is the largest root of the equation

$$1 - \left(\frac{b}{\rho} \right)^2 - \frac{U(\rho)}{E} = 0. \tag{25}$$

Physically, ρ_m corresponds to the minimum distance between two particles during their interaction. The root ρ_m is calculated by the bisection method with a numerical accuracy 10^{-15} for given values of E and b. To overcome the singularity of the integrand in Eq. (24) the integration is split as

$$\psi = \frac{b}{\rho_m} \int_0^1 \cdots \mathrm{d}q = \frac{b}{\rho_m} \left(\int_0^{1-\varepsilon} \cdots \mathrm{d}q + \int_{1-\varepsilon}^1 \cdots \mathrm{d}q \right), \tag{26}$$

where $\varepsilon \ll 1$. The first term in the parentheses of Eq. (26) is calculated using the adaptive Simpson method [31], with the numerical accuracy 10^{-15}, while the second term is approximated analytically as

$$2\sqrt{\varepsilon} \left[2 \left(\frac{b}{\rho_m} \right)^2 - \frac{\rho_m}{E} \left. \frac{\mathrm{d}U}{\mathrm{d}\rho} \right|_{\rho_m} \right]^{-1/2}. \tag{27}$$

In the numerical calculations the values of ε was 10^{-8}. Such a split allows us to calculate the deflection angle with higher accuracy than that in Ref. [27].

Once the angle ψ is known the deflection angle is calculated as

$$\chi = \arccos[-\cos(2\psi)]. \tag{28}$$

Note, the angle ψ can vary from zero to infinity, while the deflection angle χ is restricted by the interval from 0 to π. Some values of the deflection angle χ are presented in Table 1 and compared with those tabulated in Ref. [27]. It can be seen that for the most values of the energy E and impact parameter b the results reported in Ref. [27] are in a good agreement with our

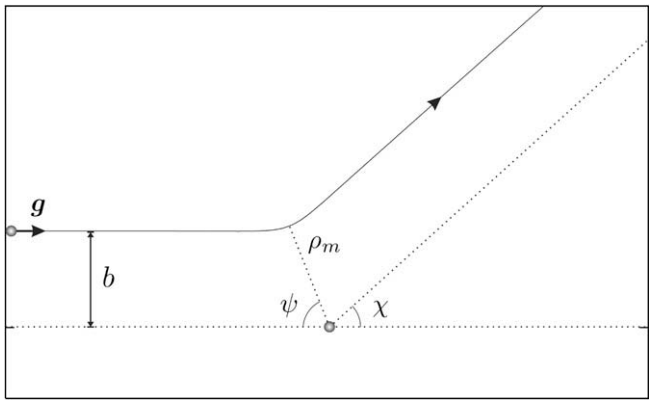

Fig. 1. Scheme and notation for binary collision.

Table 1
Deflection angle χ vs. impact parameter b for some values of energy E.

$E = 0.1$			$E = 1$			$E = 10$			$E = 100$		
b	χ		b	χ		b	χ		b	χ	
	Present	Ref. [27]		Present	Ref. [27]		Present	Ref. [27]		Present	Ref. [27]
2.838	0.3230	0.323	1.894	0.3682	0.369	1.477	0.1094	0.110	1.244	0.01961	0.020
2.696	0.5435	0.543	1.768	0.7700	0.768	1.334	0.1794	0.179	1.109	0.01309	0.013
2.643	0.7049	0.706	1.721	1.201	1.207	1.259	0.2062	0.206	1.035	0.01803	0.018
2.598	0.9437	0.945	1.698	1.683	1.689	1.205	0.1912	0.192	0.9812	0.07213	0.072
2.572	1.199	1.205	1.678	2.693	2.664	1.162	0.1402	0.141	0.9376	0.1452	0.145
2.544	1.977	1.998	1.668	3.062	3.105	1.123	0.05934	0.060	0.8990	0.2342	0.234
2.539	2.584	2.576	1.658	3.103	3.135	1.086	0.04310	0.043	0.8630	0.3361	0.336
2.538	2.903	2.346	1.643	2.699	2.784	1.049	0.1624	0.163	0.8280	0.4487	0.449
2.516	1.802	1.166	1.623	2.270	2.320	1.011	0.2943	0.297	0.7931	0.5698	0.570
2.503	2.324	1.944	1.596	1.850	1.871	0.9704	0.4389	0.440	0.7576	0.6983	0.699
2.470	3.081	2.867	1.563	1.473	1.470	0.9277	0.5905	0.592	0.7206	0.8344	0.835
2.456	2.984	3.106	1.522	1.117	1.109	0.8816	0.7505	0.752	0.6818	0.9771	0.978
2.400	2.356	2.509	1.473	0.7804	0.775	0.8315	0.9188	0.920	0.6403	1.128	1.129
2.328	1.819	1.943	1.415	0.4574	0.458	0.7762	1.097	1.099	0.5954	1.288	1.289
2.171	1.041	1.124	1.348	0.1463	0.148	0.7145	1.288	1.289	0.5461	1.459	1.460
1.996	0.4360	0.491	1.270	0.1624	0.161	0.6444	1.495	1.496	0.4908	1.646	1.646
1.881	0.1119	0.150	1.178	0.4781	0.474	0.5627	1.725	1.726	0.4272	1.854	1.854
1.593	0.5613	0.542	0.9410	1.151	1.149	0.4632	1.993	1.993	0.3507	2.096	2.097
1.119	1.444	1.437	0.5588	2.028	2.027	0.3302	2.335	2.335	0.2493	2.407	2.407

ones. However, for the small value of the energy $E = 0.1$ and for the impact parameter b varying in the interval from 2.503 to 2.539 the deflection angle calculated here is quite different from that reported in Ref. [27]. The discrepancy occurs in the range where the deflection angle χ oscillates frequently between 0 and π. Physically, this oscillation corresponds to the situation when a moving particle makes several loops around the fixed particle during their interaction. The numerical method to calculate χ described in Ref. [27] does not provide a good accuracy for such a situation. In spite of the discrepancy pointed out above its influence on integral characteristics, e.g. omega integrals, could not be so significant.

The omega integrals are defined as [26–28]

$$\Omega^{(l,r)} = \sqrt{\frac{\pi}{8}}\frac{v_m d^2}{2^r}\int_0^\infty \exp\left(-\frac{g^2}{2}\right) g^{2r+3}\int_0^{b_M}[1-\cos^l\chi(g,b)]b\,db\,dg \tag{29}$$

and widely used in the kinetic theory of gases to calculate the transport coefficients. For the hard spheres the integrals are calculated analytically

$$\Omega^{(l,r)}_{h.s.} = \sqrt{\frac{\pi}{8}}(r+1)!\left[1-\frac{1+(-1)^l}{2(l+1)}\right]v_m d^2. \tag{30}$$

Note that the numerical data on the deflection angle presented in Table 1 are given in terms of the dimensionless energy E and impact parameter b. In this case it is not necessary to specify the potential parameters ϵ and d. However, to calculate the omega integrals (29) the dependence of the deflection angle on the relative speed g is needed. According to Eqs. (13) and (16) the dimensionless relative velocity g is related to the energy E as

$$g^2 = \frac{4\epsilon}{m v_m^2}E = \frac{2\epsilon}{kT}E, \tag{31}$$

Table 2
Reduced omega integrals $\Omega^{(l,r)*}$.

	$kT/\epsilon = 0.3$		$kT/\epsilon = 1$		$kT/\epsilon = 10$	
	Present	Ref. [27]	Present	Ref. [27]	Present	Ref. [27]
$\Omega^{(1,1)*}$	2.650	2.662	1.440	1.439	0.7422	0.7424
$\Omega^{(1,2)*}$	2.257	2.256	1.204	1.204	0.7008	0.7013
$\Omega^{(1,3)*}$	1.966	1.962	1.076	1.076	0.6733	0.6735
$\Omega^{(2,2)*}$	2.844	2.785	1.593	1.587	0.8244	0.8242
$\Omega^{(2,3)*}$	2.581	2.535	1.389	1.387	0.7927	0.7922
$\Omega^{(2,4)*}$	2.362	2.333	1.259	1.258	0.7693	0.7690
$\Omega^{(2,5)*}$	2.170	2.152	1.172	1.172	0.7507	0.7501
$\Omega^{(2,6)*}$	2.001	1.990	1.113	1.113	0.7352	0.7345
$\Omega^{(4,4)*}$	2.571	2.557	1.381	1.377	0.8000	0.7988

i.e. the omega integrals depend on the reduced temperature $T^* = kT/\epsilon$.

In the literature, usually the reduced omega integrals

$$\Omega^{(l,r)*} = \frac{\Omega^{(l,r)}}{\Omega^{(l,r)}_{h.s.}} \tag{32}$$

are reported. In Ref. [27], the omega integrals are tabulated for a wide range of the parameter T^*. Here, the integrals were calculated with the accuracy 10^{-5} for three values of T^*, viz., 0.3, 1 and 10. A comparison with these data of Ref. [27] is performed in Table 2. It can be seen that the improvement of the accuracy in the deflection angle $\chi(E,b)$ did not change significantly the omega integrals.

5. Differential cross section

According to the definition, the DCS is related to the function $\chi(E,b)$ as

$$\sigma(E,\chi) = \frac{b}{\sin\chi}\frac{1}{\left|\frac{\partial\chi}{\partial b}\right|}. \tag{33}$$

However, the numerical results on the deflection angle $\chi(E,b)$ obtained here and in Ref. [27] show that there are several values of the impact parameter b corresponding to the same value of the deflection angle χ. Thus, if the energy E is fixed, then several inverse functions $b = b(E,\chi)$ will correspond to the same function $\chi = \chi(E,b)$. In this case, the DCS is related to the deflection angle as [32,33]

$$\sigma(E,\chi) = \frac{1}{\sin\chi}\sum_i b_i\left|\frac{\partial b_i(E,\chi)}{\partial\chi}\right|, \tag{34}$$

where the summing includes all inverse function $b_i = b_i(E,\chi)$.

A direct calculation of the DCS using Eq. (34) is not a simple task because the derivative $\frac{\partial b}{\partial\chi}$ can be singular. Moreover, for some values of χ and E the number of the inverse functions $b_i(E,\chi)$ can be infinite. To overcome all these problems some methods were developed [34,35] such as: expansions of σ in series, the histogram method, the method of incomplete cross section. Among these methods, the last seems the best choice, since it provides good results with a modest computational effort.

In our notations, the incomplete cross sections $W(E,\chi)$ is defined as

$$W(E,\chi) = \int_\chi^\pi \sigma(E,\chi')\sin\chi'\,\mathrm{d}\chi'. \tag{35}$$

If the function $W(E,\chi)$ is known, it is possible to calculate the DCS as

$$\sigma(E,\chi) = -\frac{1}{\sin\chi}\frac{\partial}{\partial\chi}W(E,\chi). \tag{36}$$

With help of Eqs. (34) and (35) the function $W(E,\chi)$ may be redefined in another way, which simplifies its calculation Ref. [35]

$$W(E,\chi') = \int_0^{b_M} bH[\chi(E,b)-\chi']\,\mathrm{d}b, \tag{37}$$

where $H(x)$ is the Heaviside step function.

In the numerical calculations, the impact parameter b and energy E are discretized as

$$b_k = \left(\frac{b_M}{N_b}\right)k, \quad 0 \leqslant k \leqslant N_b, \tag{38}$$

$$E_i = (E_{max}-E_{min})\left(\frac{i^2-1}{N_e^2-1}\right)+E_{min}, \quad 1 \leqslant i \leqslant N_e, \tag{39}$$

where N_b and N_e are integer. Then, the angle ψ is calculated for all pairs b_k and E_i using the procedure described above, i.e. the matrix

$$\psi_{ik} = \psi(E_i, b_k) \tag{40}$$

is stored. The variable χ is discretized as

$$\chi_j = j\Delta\chi, \quad \Delta\chi = \frac{\pi}{N_\chi}, \qquad 0 \leqslant j \leqslant N_\chi, \tag{41}$$

where N_χ is an integer. Then, the incomplete cross section $W(E_i,\chi_j)$ is calculated for all pairs E_i and χ_j as

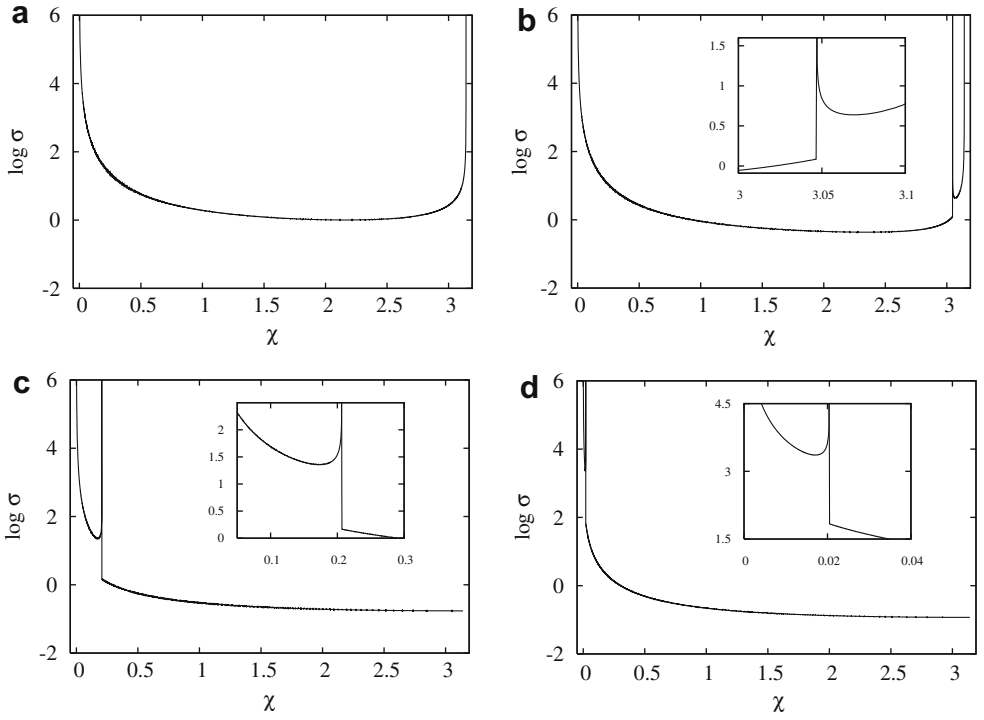

Fig. 2. Differential cross section σ vs deflection angle χ: (a) $E = 0.1$; (b) $E = 1$; (c) $E = 10$; (d) $E = 100$.

Table 3
Differential cross section σ vs deflection angle χ.

	σ			
χ	$E = 0.1$	1	10	100
0	∞	∞	∞	∞
0.01	3.73(4)[a]	1.73(4)	8.14(3)	4.88(3)
0.019792	7.77(3)	3.57(3)	1.71(3)	3.60(3)
0.020420	7.12(3)	3.29(3)	1.59(3)	∞
0.021363	6.37(3)	2.97(3)	1.42(3)	6.46(1)
0.1001	1.77(2)	8.22(2)	4.90(2)	5.921
0.2000	3.70(1)	1.73(2)	3.46(2)	1.920
0.20577	3.50(1)	1.64(2)	9.12(2)	1.834
0.20656	3.45(1)	1.62(2)	∞	1.823
0.20735	3.45(1)	1.60(2)	1.460	1.812
0.3000	1.56(1)	7.285	0.9636	1.019
0.5000	5.728	2.706	0.5583	0.4897
1.000	1.924	0.9056	0.2965	0.2196
1.200	1.542	0.7230	0.2583	0.1865
1.400	1.310	0.6102	0.2331	0.1652
1.600	1.164	0.5371	0.2152	0.1507
2.000	1.022	0.4566	0.1925	0.1329
2.200	1.008	0.4386	0.1853	0.1275
2.400	1.040	0.4351	0.1802	0.1235
2.600	1.151	0.4532	0.1764	0.1207
2.800	1.449	0.5227	0.1740	0.1189
3.000	2.713	0.8803	0.1726	0.1180
3.0461	3.783	1.211	0.1725	0.1179
3.0470	3.818	∞	0.1725	0.1178
3.0477	3.841	1.22(1)	0.1725	0.1178
3.14	1.989(2)	1.405(2)	0.1724	0.1178
π	∞	∞	0.1724	0.1178

[a] Numbers in parentheses indicate the power of 10 by which the corresponding entry is to be multiplied.

$$W_{ij} = W(E_i, \chi_j) = \frac{b_M}{N_c} \sum_{n=1}^{N_c} b_n H[\chi(E_i, b_n) - \chi_j], \quad b_n = \frac{b_M}{N_c}\left(n - \frac{1}{2}\right), \tag{42}$$

where $\chi(E_i, b_n)$ is related to $\psi(E_i, b_n)$ by Eq. (28). The values of $\psi(E_i, b_n)$ were obtained from a quadratic polynomial interpolation of the matrix ψ_{ik} calculated previously.

Now, using Eq. (36) the values $\sigma(E_i, \chi_j)$ are approximated by

$$\sigma(E_i, \chi_j) = -\frac{1}{\sin\chi_j} \begin{cases} \frac{W_{i1} - W_{i0}}{\Delta\chi} & \text{if } j = 0, \\ \frac{W_{ij+1} - W_{ij-1}}{2\Delta\chi} & \text{if } 0 < j < N_\chi, \\ \frac{W_{iN_\chi} - W_{iN_\chi - 1}}{\Delta\chi} & \text{if } j = N_\chi. \end{cases} \tag{43}$$

The calculation of the DCS was carried out using the following parameters $b_M = 20, E_{min} = 10^{-3}, E_{max} = 10^3, N_b = 10^5$ and $N_c = 10^8, N_e = 4000, N_\chi = 5000$. In the most part of the variation interval of the deflection angle, the relative accuracy is 0.1% estimated by a comparison of results obtained for different values of the numerical scheme parameters. Near the singularities, i.e. when $\sigma(E, \chi) \to \infty$, the relative error is larger and reaches 2% in few points. However, such an inaccuracy causes the relative uncertainty in the final numerical results on the transport coefficients within 10^{-4}.

For four values of the energy, i.e. $E = 0.1$, 1, 10 and 100, the DCS is plotted in Fig. 2. It can be seen that for the small energy value ($E = 0.1$) the function $\sigma(E, \chi)$ is smooth. However, for the intermediate ($E = 1$) and large values ($E = 10$ and 100) of the energy, the DCS represents very narrow peaks tending to infinity. Such kind of the behaviour was indicated in the scattering theory, see e.g. Ref. [33]. They are related to the fact that the derivatives $\partial\chi/\partial b$ are zero in the corresponding points. It should be noted that the curves are smooth on one side of the peaks, while they are broken on the other side. The numerical data of the DCS are also reported in Table 3 where the peak positions and nearest points are included.

6. Transport coefficients

6.1. General remarks

When the DCS is known, the kernel (19) can be calculated and then the integro-differential Eq. (17) can be solved. To solve such kind of kinetic equation, usually the discrete velocity method [2] is applied. First, a mesh in the velocity space is chosen and the collision operator (23) is expressed by some quadrature formula. The left hand side of Eq. (17) is approximated by some finite difference scheme. Then, using an iterative procedure the perturbation function $h(\boldsymbol{r}, \boldsymbol{c})$ is calculated in all points of the physical space for all points of the velocity space. Once the perturbation function is known, any macroscopic quantity can be calculated.

The optimum choice of the mesh in the velocity space is crucial for a successful solution of rarefied gas problems. The mesh must be sufficiently dense to provide a good accuracy, but with a reasonable computational effort. In order to find an optimum mesh and to estimate the computational effort needed to solve the kinetic equation, the transport coefficients, viz. thermal conductivity and viscosity, are calculated in this section. This problem is zero-dimensional and does not require any finite difference scheme. The transport coefficients calculated directly from the kinetic equation will be compared with those obtained by the variational method in the frame of the Chapman–Enskog expansion.

6.2. Integral equation

According to Ref. [26–28] the heat conductivity κ' and viscosity μ' coefficients are calculated as

$$\kappa' = \frac{k\nu_m}{d^2} \int \phi(\boldsymbol{c}) A(c) c_x^2 \left(c^2 - \frac{5}{2}\right) \mathrm{d}\boldsymbol{c}, \tag{44}$$

$$\mu' = \frac{m\nu_m}{d^2} \int \phi(\boldsymbol{c}) B(c) (c_x c_y)^2 \, \mathrm{d}\boldsymbol{c}, \tag{45}$$

respectively. The functions $A(c)$ and $B(c)$ satisfy the corresponding integral equations

$$\widehat{L}[A(c)c_x] + c_x\left(c^2 - \frac{5}{2}\right) = 0, \tag{46}$$

$$\widehat{L}[B(c)c_x c_y] + 2c_x c_y = 0. \tag{47}$$

In accordance with Eq. (21), the quantity c_x is a collision invariant. As a consequence, the integral Eq. (46) does not determine the function $A(c)$ completely, but an additional constraint is necessary. Assuming that the gas must be at rest, such a constraint reads as

$$\int \phi(\boldsymbol{c}) A(c) c_x^2 \, \mathrm{d}\boldsymbol{c} = 0. \tag{48}$$

Following Ref. [16] it is possible to simplify the numerical solution eliminating one variable in the velocity space. Let us introduce the cylindrical coordinates

$$\boldsymbol{c} = (c_x, c_y, c_z) = (c_x, c_r\cos\theta, c_r\sin\theta). \tag{49}$$

From Eq. (46) we conclude that the solution does not depend from the angle θ, but it depends only on c_x and c_r. Then, the integral Eq. (46) is reduced to

$$\widehat{L}_1[A(c)c_x] + c_x\left(c^2 - \frac{5}{2}\right) = 0, \tag{50}$$

where

$$\widehat{L}_1(h) = \int_{-\infty}^{+\infty}\int_0^{+\infty} \phi(\boldsymbol{c}^*)K_1(c_x, c_r, c_x^*, c_r^*)\left[h(c_x^*, c_r^*) - h(c_x, c_r)\right]c_r^*\,\mathrm{d}c_r^*\,\mathrm{d}c_x^*, \tag{51}$$

which is obtained from Eq. (23) with $\Psi = 1$. Note, the function $\phi(\boldsymbol{c})$ does not depend from the angle θ. The kernel K_1 is given by

$$K_1(c_x, c_r, c_x^*, c_r^*) = 2\int_0^{\pi} K(c_x, c_r, c_x^*, c_r^*, \beta)\,\mathrm{d}\beta, \quad \beta = \theta^* - \theta. \tag{52}$$

As was pointed out in Ref. [14], Eq. (47) can be written as

$$\widehat{L}_2[B(c)c_x] + 2c_xc_r = 0, \tag{53}$$

where the operator $\widehat{L}_2$ is obtained from Eq. (23) with $\Psi = c_y$

$$\widehat{L}_2(h) = \int_{-\infty}^{+\infty}\int_0^{+\infty} \phi(\boldsymbol{c}^*)K_2(c_x, c_r, c_x^*, c_r^*)\left[h(c_x^*, c_r^*) - h(c_x, c_r)\right]c_r^{*2}\,\mathrm{d}c_r^*\,\mathrm{d}c_x^*. \tag{54}$$

The kernel K_2 reads

$$K_2(c_x, c_r, c_x^*, c_r^*) = 2\int_0^{\pi} K(c_x, c_r, c_x^*, c_r^*, \beta)\cos\beta\,\mathrm{d}\beta, \quad \beta = \theta - \theta^*. \tag{55}$$

Then, the calculation of the viscosity is reduced to the solution of Eq. (53).

It is convenient to present the numerical results in terms of the reduced transport coefficients defined as

$$\kappa = \kappa'\frac{d^2}{k\upsilon_m} = \int \phi(\boldsymbol{c})A(c)c_x^2\left(c^2 - \frac{5}{2}\right)\mathrm{d}\boldsymbol{c}, \tag{56}$$

$$\mu = \mu'\frac{d^2}{m\upsilon_m} = \int \phi(\boldsymbol{c})B(c)(c_xc_y)^2\,\mathrm{d}\boldsymbol{c}. \tag{57}$$

6.3. Variational solution

In Refs. [26–28] a variational method to solve Eqs. (46) and (47) was applied. The trial functions were presented as series of Sonine polynomials. Finally, the transport coefficients were expressed via the omega integrals (29), which depend on the reduced temperature $T^* = kT/\epsilon$.

In the open literature, one can find diverse data, see e.g. Ref. [27], on the parameters ϵ and d, which were extracted from experimental data. Since our aim is the elaboration of numerical procedure to solve the kinetic equation, any data can be used for our test. In this section, the numerical procedure will be applied to calculate the transport coefficients, that is why the data extracted from the viscosity coefficient reported in Table I-A of Ref. [27] are used in the present work. The values of ϵ and d corresponding to the noble gases used here are given in Table 4.

The omega integrals needed to calculate the transport coefficients were calculated on the basis of the numerical data on the deflection angle $\chi(E, b)$ presented in Section 4 assuming $T = 300$ K and using the values of ϵ from Table 4. Then, the

Table 4
Lennard-Jones parameters for noble gases, Ref. [27].

Gas	ϵ/k (K)	d (nm)
He	10.22	0.2576
Ne	35.7	0.2789
Ar	124	0.3418
Kr	190	0.361
Xe	229	0.4055

Table 5
Reduced heat conductivity κ obtained by the variational method and by the discrete velocity (DV) method.

Gas	Variational method			DV method
	$\kappa^{(1)}$	$\kappa^{(2)}$	$\kappa^{(3)}$	κ
He	0.66499	0.67264	0.67320	0.6740
Ne	0.55388	0.55982	0.56018	0.5600
Ar	0.42335	0.42479	0.42479	0.4260
Kr	0.36321	0.36346	0.36349	0.3645
Xe	0.33476	0.33481	0.33485	0.3358

Table 6
Reduced viscosity μ obtained by the variational method and by the discrete velocity (DV) method.

Gas	Variational method			DV method
	$\mu^{(1)}$	$\mu^{(2)}$	$\mu^{(3)}$	μ
He	0.17733	0.17866	0.17873	0.1787
Ne	0.14770	0.14873	0.14878	0.1480
Ar	0.11289	0.11314	0.11314	0.1130
Kr	0.096855	0.096899	0.096902	0.09680
Xe	0.089269	0.089278	0.089282	0.08919

viscosity and heat conductivity were calculated using the analytical expressions (7.3-7) and (7.3-18) in Ref. [28], respectively. These expressions represent 3rd order Chapman–Cowling approximation. The values of transport coefficients κ and μ for the three approximations are given in Tables 5 and 6, respectively. It can be seen that the third approximation provides a good convergence. Below, these data will be used as benchmark values for the direct solution of the integral equations (50) and (53).

6.4. Numerical mesh in the velocity space

To apply the discrete velocity method to both (50) and (53) a mesh in the two dimensional velocity space, i.e. (c_x, c_r) must be introduced. Several node distributions were tested and the following was chosen as the optimum one. The velocity components were restricted by the intervals $0 \leqslant |c_x| \leqslant 5$ and $0 \leqslant c_r \leqslant 5$. The positive axis of c_x is divided in non-regular subintervals as

$$\Delta c_{xk} = 5\left(\frac{5k}{N_{cx}}\right)^{1.8}\left[1-\left(\frac{k-1}{k}\right)^{1.8}\right], \quad 1 \leqslant k \leqslant \frac{N_{cx}}{5}, \tag{58}$$

while the variable c_r is divided in regular subintervals

$$\Delta c_r = \frac{25}{N_{cr}}, \tag{59}$$

where N_{cx} and N_{cr} are integer. In each subinterval, the nodes and weights of the Gauss–Legendre quadrature with five points is used. Thus, each node c_{xk} or c_{rk} has its own weight W_{xk} or W_{rk}, respectively. The negative points of the variable c_x are distributed symmetrically with respect to the origin so as

$$c_{x,-k} = -c_{xk}, \quad W_{x,-k} = W_{x,k}, \quad 1 \leqslant k \leqslant N_{cx}. \tag{60}$$

6.5. Numerical scheme for the heat conductivity

Let us denote the unknown values of the function $A(c)c_x$ in the mesh points as

$$X_{km} = A(c_{km})c_{xk}, \quad c_{km} = \sqrt{c_{xk}^2 + c_{rm}^2}. \tag{61}$$

Then, the integral equation (50) is discretized as

$$\sum_{i,j} \mathcal{L}_{ijkm}(X_{ij} - X_{km}) + \mathcal{S}_{km} = 0, \tag{62}$$

where

$$\mathcal{L}_{ijkm} = \phi(c_{ij})K_1(c_{xk}, c_{rm}, c_{xi}, c_{rj})c_{rj}W_{xi}W_{rj}, \tag{63}$$

$$\mathcal{S}_{km} = c_{xk}\left(c_{km}^2 - \frac{5}{2}\right), \tag{64}$$

$$-N_{cx} \leqslant i, \quad k \leqslant -1, \quad 1 \leqslant i, k \leqslant N_{cx}, \tag{65}$$

$$1 \leqslant j, \quad m \leqslant N_{cr}. \tag{66}$$

So, the integral equation (50) is reduced to the linear algebraic equation (62), which is solved by an iterative procedure. The result of each iteration must be corrected using the condition (48). The correction of nth iteration is calculated as

$$D^{(n)} = 4\pi \sum_{k,m} \phi(c_{km})\tilde{X}_{km}c_{xk}c_{rm}W_{xk}W_{rm}, \tag{67}$$

which is subtracted from $X_{km}^{(n)}$. Finally, the iterative procedure takes the form

$$\tilde{X}_{km}^{(n)} = X_{km}^{(n-1)} + \frac{1}{\nu_{km}}\left[\sum_{i,j}\mathcal{L}_{ijkm}\left(X_{ij}^{(n-1)} - X_{km}^{(n-1)}\right) + \mathcal{S}_{km}\right], \tag{68}$$

$$X_{km}^{(n)} = \tilde{X}_{km}^{(n)} - D_{c_{xk}}^{(n)}, \tag{69}$$

where

$$\nu_{km} = \nu(c_{km}), \tag{70}$$

$\nu(c)$ is given by Eq. (20). The reduced thermal conductivity coefficient $\kappa^{(n)}$ is calculated at each iteration as

$$\kappa^{(n)} = 2\pi \sum_{k,m} \phi(c_{km})X_{km}^{(n)}\left(c_{km}^2 - \frac{5}{2}\right)c_{xk}c_{rm}W_{xk}W_{rm}. \tag{71}$$

The iteration is stopped when the relative difference of the heat conductivity in two successive iterations does not exceed the value 10^{-8}.

6.6. Numerical scheme for the viscosity

Let us denote the unknown values of the function $B(c)c_x$ in the mesh points as

$$X_{km} = B(c_{km})c_{xk}. \tag{72}$$

Then, the integral equation (53) is discretized exactly as in the previous case, i.e. by Eq. (62), with the difference that

$$\mathcal{L}_{ijkm} = \phi(c_{ij})K_2(c_{xk}, c_{rm}, c_{xi}, c_{rj})c_{rj}^2W_{xi}W_{rj}, \tag{73}$$

$$\mathcal{S}_{km} = 2c_{xk}c_{rm}. \tag{74}$$

Finally, the iterative procedure takes the form

$$X_{km}^{(n)} = X_{km}^{(n-1)} + \frac{1}{\nu_{km}}\left[\sum_{i,j}\mathcal{L}_{ijkm}\left(X_{ij}^{(n-1)} - X_{km}^{(n-1)}\right) + \mathcal{S}_{km}\right]. \tag{75}$$

The reduce viscosity coefficient μ is calculated in each iteration as

$$\mu^{(n)} = \pi \sum_{k,m} \phi(c_{km})X_{km}^{(n)}c_{xk}c_{rm}^3W_{xk}W_{rm}. \tag{76}$$

The iteration is stopped when the relative difference of the viscosity in two successive iterations does not exceed the value 10^{-8}.

6.7. Results and discussion

First, the numerical calculations were carried out for the hard sphere molecules with the DCS given by Eq. (9). For this potential the papers [6–9,18] reported the following values of the reduced transport coefficients

$$\kappa = 0.479305, \quad \mu = 0.126668 \tag{77}$$

obtained by different methods. In the present work, the numbers of nodes $N_{cx} = 40$ and $N_{cr} = 40$ were used to discretized the component c_x and c_r, respectively. To calculate the integrals (52) and (55) the Simpson quadrature was used with 200 points. As a results the values

$$\kappa = 0.47928, \quad \mu = 0.126668 \tag{78}$$

were obtained, i.e. the relative difference of the heat conductivity from the previously obtained result does not exceed 5×10^{-5}, while the value of the viscosity is the same within the six digits.

The same mesh in the velocity space was applied to the calculation of the heat conductivity κ and viscosity μ using the Lennard-Jones potential with the parameters given in Table 4 for all noble gases. The numerical results are given in Tables 5 and 6 for κ and μ, respectively. It can be seen that they are in a good agreement with those obtained by the variational method described in Refs. [26–28]. The maximum relative discrepancy does not exceed 5×10^{-3}.

It should be noted that the reduced transport coefficients κ and μ for the Lennard-Jones potential depend only on the parameter ϵ. The other parameter d is used only to related the reduced coefficients to the corresponding dimensional ones by Eqs. (56) and (57). According to Table 4 the parameter ϵ/k is quite different for different gas species and varies from 10.22 K to 229 K. However, the variation of the reduced coefficients κ and μ is not so significant. Their maximum values are about double of their minimum ones.

7. Concluding remarks

The numerical scheme to solve the linearized Boltzmann equation for an arbitrary intermolecular potential was proposed. As an example of its application, the thermal conductivity and viscosity coefficients were calculated. First, the scheme was tested for the hard sphere model. A comparison with previously obtained numerical results showed that the relative numerical error for the heat conductivity does not exceed 5×10^{-5}, while the viscosity was calculated with the accuracy of six digits. Then, both thermal conductivity and viscosity were calculated for the nobles gases using the Lennard-Jones potential. These are the first results based on the direct numerical solution of the linearized Boltzmann equation. They were compared with those obtained by the variational method based on the approximation of the perturbation function by the Sonine polynomials. The discrepancy between the present results and approximated ones does not exceed 5×10^{-3}.

The main computational effort to solve the Boltzmann equation for an arbitrary potential is concentrated in calculations of the kernel, which depends on the mesh in the velocity space. Fortunately, the kernel does not depend on the mesh in the physical space. Hence, once the kernel is calculated and stored it can be used to solve several problems of rarefied gas dynamics with an additional effort, which is not significant.

In forthcoming papers, results for classical rarefied gas flows based on the kernel calculated in the present paper will be reported.

Acknowledgments

The authors acknowledge the Conselho Nacional de Desenvolvimento Científico e Tecnológico (CNPq, Brazil) for the support of their research.

References

[1] E.M. Shakhov, Method of Investigation of Rarefied Gas Flows, Nauka, Moscow, 1974 (in Russian).
[2] F. Sharipov, V. Seleznev, Data on internal rarefied gas flows, J. Phys. Chem. Ref. Data 27 (3) (1998) 657–706.
[3] Y. Sone, Molecular Gas Dynamics Theory Techniques and Applications, Birkhäuser, Boston, 2007.
[4] C. Cercignani, Slow Rarefied Flows: Theory and Application to Micro-Electro-Mechanical Systems, Birkhäuser Verlag, Basel, 2006.
[5] G.A. Bird, Molecular Gas Dynamics and the Direct Simulation of Gas Flows, Oxford University Press, Oxford, 1994.
[6] C.L. Pekeris, Z. Alterman, Solution of the Boltzmann–Hilbert integral equation. II: the coefficients of viscosity and heat conduction, Proc. Natl. Acad. Sci. 43 (1957) 998–1007.
[7] C. Siewert, On computing the Chapman–Enskog functions for viscosity and heat transfer and the Burnett functions, J. Quant. Spectr. Rad. Transfer 74 (6) (2002) 789–796.
[8] L.B. Barichello, P. Rodrigues, C.E. Siewert, On computing the Chapman–Enskog and Burnett functions, J. Quant. Spectr. Rad. Transfer 86 (2004) 109–114.
[9] A. Mohan, R.V. Tompson, K.A. Hickey, S.K. Loyalka, Chapman–Enskog and Burnett solutions for a simple rigid-sphere gas: numerical solutions using a subtraction technique, J. Quant. Spectr. Rad. Transfer 109 (5) (2008) 741–751.
[10] S.K. Loyalka, Temperature jump and thermal creep slip: rigid sphere gas, Phys. Fluids A 1 (1989) 403–408.
[11] S.K. Loyalka, K.A. Hickey, Velocity slip and defect: hard sphere gas, Phys. Fluids A 1 (3) (1989) 612–614.
[12] S.K. Loyalka, K.A. Hickey, Plane Poiseuille flow: near continuum results for rigid sphere gas, Physica A 160 (1989) 395–408.
[13] T. Ohwada, Y. Sone, K. Aoki, Numerical analysis of the Poiseuille thermal transpiration flows between two parallel plates on the basis of the Boltzmann equation for hard sphere molecules, Phys. Fluids A 1 (12) (1989) 2042–2049.
[14] T. Ohwada, Y. Sone, K. Aoki, Numerical analysis of the shear and thermal creep flows of a rarefied gas over a plane wall on the basis of the linearized Boltzmann equation for hard-sphere molecules, Phys. Fluids A 1 (9) (1989) 1588–1599.
[15] T. Ohwada, K. Aoki, Y. Sone, Heat transfer and temperature distribution in a rarefied gas between two parallel plates with different temperatures: numerical analysis of the Boltzmann equation for a hard sphere molecule, in: E.P. Muntz, D.P. Weaver, D.H. Campbell (Eds.), Rarefied Gas Dynamics: Theoretical and Computational Techniques, 20st Int. Symp., China, 1996, AIAA, Washington, 1989, pp. 70–81.
[16] Y. Sone, T. Ohwada, K. Aoki, Temperature jump and Knudsen layer in a rarefied gas over a plane wall: numerical analysis of the linearized Boltzmann equation for hard-sphere molecules, Phys. Fluids A 1 (2) (1989) 363–370.
[17] Y. Sone, S. Takata, T. Ohwada, Numerical analysis of the plane Couette flow of a rarefied gas on the basis of the linearized Boltzmann equation for hard-sphere molecules, Eur. J. Mech. B – Fluids 9 (3) (1990) 273–288.
[18] T. Ohwada, Y. Sone, Analysis of thermal-stress slip-flow and negative thermophoresis using the Boltzmann equation for hard-sphere molecules, Eur. J. Mech. B – Fluids 11 (4) (1992) 389–414.
[19] S. Takata, Y. Sone, K. Aoki, Numerical analysis of a uniform flow of a rarefied gas past a sphere on the basis of the Boltzmann equation for hard-sphere molecules, Phys. Fluids A 5 (3) (1993) 716–737.
[20] M. Wakabayashi, T. Ohwada, F. Golse, Numerical analysis of the shear and thermal creep flows of a rarefied gas over the plane wall of a Maxwell-type boundary on the basis of the linearized Boltzmann equation for hard-sphere molecules, Eur. J. Mech. B – Fluids 15 (2) (1996) 175–201.

[21] C.E. Siewert, The linearized Boltzmann equation: a concise and accurate solution of the temperature-jump problem, J. Quant. Specr. Rad. Transfer 77 (2003) 417–432.
[22] C.E. Siewert, The linearized Boltzmann equation: concise and accurate solutions to basic flow problems, Z. Angew. Math. Phys. (ZAMP) 54 (2003) 273–303.
[23] C.E. Siewert, Viscous-slip, thermal-slip and temperature-jump coefficients as defined by the linearized Boltzmann equation and the Cercignani–Lampis boundary condition, Phys. Fluids 15 (6) (2003) 1696–1701.
[24] S.K. Loyalka, Slip and jump coefficients for rarefied gas flows: variational results for Lennard-Jones and $n(r) - 6$ potential, Physica A 163 (1990) 813–821.
[25] F. Sharipov, Application of the Cercignani–Lampis scattering kernel to calculations of rarefied gas flows. II. Slip and jump coefficients, Eur. J. Mech. B – Fluids 22 (2003) 133–143.
[26] S. Chapman, T.G. Cowling, The Mathematical Theory of Non-Uniform Gases, University Press, Cambridge, 1952.
[27] J. Hirschfelder, C. Curtiss, R. Bird, The Molecular Theory of Gases and Liquids, Wiley, New York, 1954.
[28] J.H. Ferziger, H.G. Kaper, Mathematical Theory of Transport Processes in Gases, North-Holland Publishing Company, Amsterdam, 1972.
[29] C. Cercignani, The Boltzmann Equation and its Application, Springer-Verlag, New York, 1988.
[30] W.H. Press, B.P. Flannery, S.A. Teukolsky, W.T. Vetterling, Numerical Recipes in FORTRAN 77: The Art of Scientific Computing, second ed., Cambridge University Press, 1992.
[31] R.L. Burden, J.D. Faires, Numerical Analysis, eighth ed., Brooks/Cole, 2004.
[32] H. Goldstein, Classical Mechanics, Addison-Wesley, 1980.
[33] H.M. Nussenzveig, Diffraction Effects in Semiclassical Scattering, Cambridge University Press, 1992.
[34] E.A. Gislason, J.G. Sachs, Expansion of classical differential cross-sections in Legendre polynomials – nonreactive scattering, Chem. Phys. 33 (3) (1978) 415–422.
[35] E.A. Gislason, Evaluation of classical differential cross-sections – simplifying methods, Chem. Phys. Lett. 42 (2) (1976) 315–318.